# Core Follow Calculation for Hanbit Unit 1 in Cycles 1 through 7 using DeCART2D/MASTER

Yonghee Choi*, Hee Jeong Jeong, Cheonbo Shim and Kyunghoon Lee
*Korea Atomic Energy Research Institute, 111, Daedeok-daero 989beon-gil, Yuseong-gu, Daejeon, 34057, Korea*
**Corresponding author: yhchoi@kaeri.re.kr*

## 1. Introduction

The DeCART2D[1]/MASTER[2] codes system has been developed in KAERI for the PWR (Pressurized water reactors) core design including SMRs (Small Modular Reactors). The DeCART2D solves the Boltzmann transport equation by Method of Characteristic (MOC) so that it generates assembly-wise homogenized and group condensed effective cross section data used in MASTER. MASTER solves the neutron diffusion equation with microscopic and macroscopic cross sections provided by the DeCART2D code. It has a variety of capabilities such as static core design or transient core analysis.

To assess the accuracy and performance of the DeCART2D/MASTER codes system, the core follow calculation for Hanbit NPP (Nuclear Power Plant) unit 1 is performed and the resulting solutions are compared with the measurement data.

The overall procedure for the calculation which will be described in subsequent chapters is divided into two steps. As the first step, the HGCs (Homogenized Group Constants) for each fuel assembly and reflector of Hanbit NPP unit 1 are prepared by using DeCART2D. After then, MASTER performs the core follow calculation with HGCs produced by DeCART2D. Since the output formats of DeCART2D are not adequate for MASTER, the edit program named PROLOG[3] is used to convert the output of DeCART2D into the specific library form of MASTER.

## 2. Generation of HGC

### *2.1 Overall description of the core*

The reactor core of Hanbit NPP unit 1 consists of 157 fuel assemblies. The fuel assembly is composed of a 17x17 array of 264 fuel rods, 24 guide tubes and one instrumentation tube as shown in Fig. 1.

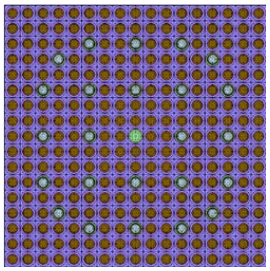

Fig. 1. Basic geometry of fuel assembly of Hanbit NPP unit 1

The fuel rods are made up of UO2 pellet slightly enriched in U235 and stacked in Zircaloy-4 tubes. The guide tube allows replacing of fuel rod with control rod. The guide tubes not containing control rod have burnable absorber rod or coolant flow.

The measurement data came from the reactor operation in which the number of the reloading cycles is 7. So the corresponding core follow calculations were also performed over the course of total 7 cycles. During the operation of cycle 1~4, the type of fuel assembly named WOFA (Westinghouse Optimized Fuel Assembly) are installed, while the cores of cycle 5~7 are arranged by KOFA (Korea Optimized Fuel Assembly). The dimension of the pin cell geometry of KOFA is different from WOFA as given in Fig. 2.

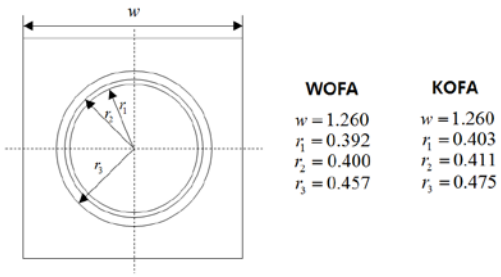


Fig. 2. Pin cell geometries of fuel rods for WOFA and KOFA in centimeter unit. Given values in the figure are nominal, while the built-in values are used in actual DeCART2D calculations. r1, r2, r3 represent the diameter of pellet, inner cladding and outer cladding and w stands for pin pitch.

As a control rod material, $B_4C$ and Hf had been used in cycle 1~6, while they were partly altered to AGINCD (Ag+In+Cd) material after cycle 7. The burnable absorbers such as $Al_2O_3$, $B_4C$ or $Gd_2O_3$ were adopted for the partial control of excess reactivity.

Total 21 types of fuel assemblies were installed in Hanbit NPP unit 1 during the operation in cycle 1 through 7. The type of assembly is mainly determined by whether it is a WOFA or KOFA due to their difference in dimension of pin cell geometry. However, it is further classified by the number or positions of the burnable absorbers and the enrichment of the fuel rods.

### *2.2 HGCs for fuel assemblies*

To obtain assembly-wise HGCs, each assembly is modeled radially and 2-D transport calculations are performed by DeCART2D with the zero net current boundary condition. The following computational options are used for HGC generation.

- 47/18 neutron/gamma energy group XS library based on the ENDF/B-VII.1
- 0.02 cm ray spacing, 8 azimuthal angles in 90° domain and 3 polar angles in 90° domain for ray discretization.
- Subgroup method for resonance treatment
- Transport correction based anisotropic scattering treatment

Owing to the symmetry, the fuel assemblies are modeled only for 1/8 part as shown in Fig. 3. The mesh division of the calculations for the fuel rods and guide tubes are also denoted in Fig. 3.

On the other hand, the cross section changes with the change of state parameters of the core. Burnup, fuel temperature, soluble boron concentration in moderator and coolant density are chosen as state parameters representing the core state in the calculation. Then, the homogenized cross section of each fuel assembly is functionalized to such variables by using branch calculations. The structure of the branch calculation adopted in this paper is given in Table I.

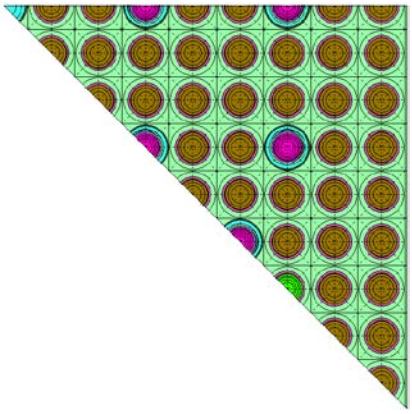

Fig. 3. 1/8 fuel assembly model used in generation of the homogenized cross section. The lines denote the computational mesh division.

Table I: Structure of the branch calculation for HGC of fuel assembly

| Control rod configuration | Variation | Remark (Variation from reference) |
|---|---|---|
| w/o control rod | Reference case | |
| | Soluble boron | +1000ppm |
| | Fuel temperature | +100K |
| | Moderator density changes by temperature variations | +20,-20, -50,-100, -180,-290 (in K unit from the reference, 310K) |
| w/ Control rod | Reference case | Same calculations are repeated for B4C, Hf, AGINCD |
| | Soluble boron | |
| | Moderator density | |

*2.3 Radial reflector cross section*

The radial reflector region is composed of a shroud, water and baffle which are surrounding the core radially. For convenience, it is supposed that the region is represented by regular arrangement of assemblies having the same dimensions and geometries with the fuel assembly. The effective cross sections of those radial reflector assemblies are generated by modeling of 1/8 core as shown in Fig. 4.

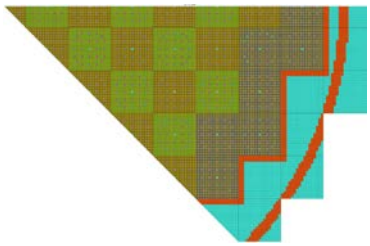

Fig. 4. 1/8 core used in radial reflector generation and the arrangement of radial reflector

Three types of radial reflector assemblies denoted by R1, R2 and R3 are introduced depending on how many fuel assemblies exist in the neighborhood. Unlike the fuel assembly, the radial reflector is assumed to be independent of burnup and fuel temperature. Instead, it is supposed that the effective cross section of radial reflector is a function of boron concentration.

*2.4 Axial reflector cross section*

The axial reflector cross sections are produced by employing a simplified 1D core model [4] as shown in Fig. 5. The top and bottom nodes of the figure stand for the top and bottom reflector assemblies respectively.

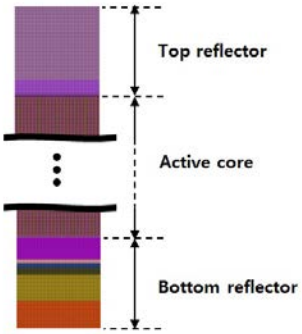


Fig. 5. Schematic figure for the simplified 1-D axial reflector model for Hanbit NPP unit 1. HGCs for top and bottom reflector are generated through this model.

In this 1-D axial core, the active core region is modeled by repetitive arrangement of fuel rod and moderator along the z-axis. The core average enrichment of UO2 is used as that of fuel pin in active core and the dimensions of geometry is adjusted to preserve the volume ratio of the original fuel and moderator.

## 3. Core follow calculations

The core follow calculations were done by MASTER with the cross section data obtained from the previous chapters. And then comparisons were made between measurement data and calculation results of MASTER for Hanbit NPP Unit 1 from cycles 1 through 7.

The target parameters to be compared include global parameters such as boron concentrations, isothermal temperature coefficient (ITC), hot full power (HFP) reactivity as well as local one like region-wise reaction rates at incore detectors. Note that the comparisons are not presented here in case that the measurement data are not fully available for whole cycles.

### *3.1 End-point boron concentration*

End-point boron concentrations are critical boron concentrations (CBC) with each individual control rod and shutdown bank inserted. However, because the measurement data are not available for all cycles other than ARO condition, only the comparison in CBC at BOC and HZP, ARO condition are given in Table II. It shows that the maximum difference occurs at cycle 7 in which the value of difference is 55 ppm.

Table II: Difference in end-point boron concentrations at BOC under the condition of HZP and ARO

| Cycle | Difference in CBC (ppm) | Relative error (%) |
|---|---|---|
| 1 | -10 | -0.83 |
| 2 | -8 | -0.64 |
| 3 | 1 | 0.07 |
| 4 | 15 | 1.06 |
| 5 | 31 | 2.07 |
| 6 | -22 | -1.38 |
| 7 | -55 | -2.89 |

### *3.2 Isothermal temperature coefficient*

If the moderator and fuel temperature changes are the same throughout the core, the temperature effect on the reactivity can be expressed by ITC defined as the change in reactivity due to change in temperature. The ITC is only measured under a condition such that the temperatures of the coolant and the fuel are identical. So ITC is regarded as one of the startup parameters measured and provided in BOC. Table III illustrates the differences in ITC between measured data and calculation results. According to it, the maximum difference in ITC is -0.87 ppm/ ℃ at cycle 3. Note that in terms of the relative error, the difference is -152.63% where it is extremely high because the signs of the measurement data and the calculation result differ.

### *3.3 HFP reactivity*

The soluble boron concentration is used as a mean of reactivity measurement in such a way that the reactivity of the core is estimated by CBC multiplied by boron worth at each burnup step. The way of reactivity estimation implies that the difference in reactivity is actually identical to the difference in CBC. The calculated results of CBC are given in Fig. 6.

Table III: Differences in ITC between measurement and calculation at BOC

| Cycle | Difference in ITC (pcm/°C) | Relative error[1)] (%) |
|---|---|---|
| 1 | -0.01 | -0.15 |
| 2 | 0.17 | -9.83 |
| 3 | -0.87 | -152.63[2)] |
| 4 | 0.24 | 21.24 |
| 5 | 0.23 | 19.17 |
| 6 | 0.18 | -16.82 |
| 7 | -0.59 | -31.22 |

1) Relative error=(calculation-measurement)/measurement
2) In this case, the signs are different such that the measurement is 0.57, while the calculation is -0.3.

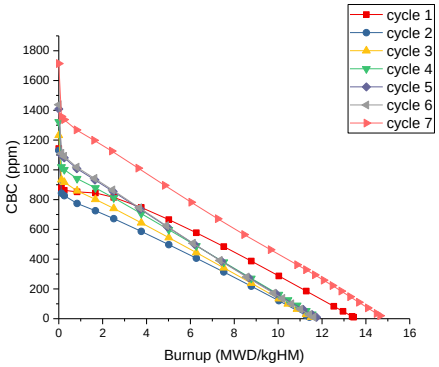


Fig. 6. CBC calculated by MASTER at each burnup step for every cycle

The Figure 7 shows the accumulated records of the differences in reactivities between measurement data and calculation results for all cycles. Among the compared results, the maximum difference in reactivity appears at cycle 1 by 466.1 pcm.

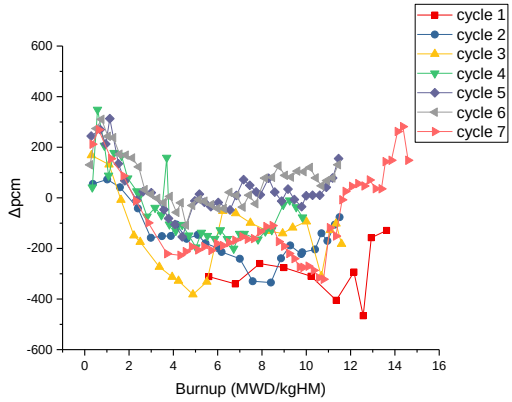


Fig. 7. Differences in reactivities between measurements and calculations at each burnup step for every cycle

### *3.4 Reaction rates at incore detectors*

Unlike the parameters such as boron concentration and temperature coefficient, the reaction rate at incore detector stands for local parameter because the response of incore detector is recorded at a specific position. During normal operation, each detector is used to measure the relative neutron flux density in the core. It means that the target of comparison in this case is the relative neutron flux density.

Comparisons are made at various cycles and burnup steps. For quantification of the uncertainty, Shapiro-Wilk normality test are applied to the observed samples. For example, Fig. 8 shows the distribution of observed differences at each incore detectors at cycle 1 and 11400MWD/MTU burnup step. In the Shapiro-Wilk hypothesis test, the null hypothesis is assumed such that the given distribution is normal. Since the p-value stands for the probability of error in case that the null hypothesis is rejected, the higher its value, the higher it supports the null hypothesis. As given in Table IV, its p-value is 31.2% and it can be considered to be very high compared to the typical value for rejection.

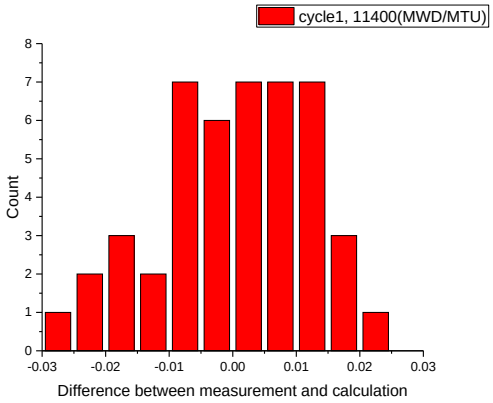


Fig. 8. Distribution of difference in relative neutron flux between measurements and calculations at cycle 1, 11400MWD/MTU

Table IV: Shapiro-Wilk test for observed differences in cycle 1 at each burnup step

| Cycle 1 | burnup (MWD/MTU) | p-value (%) |
|---|---|---|
| 1 | 1712 | 25.2 |
| 1 | 6300 | 20.1 |
| 1 | 8800 | 61.2 |
| 1 | 11000 | 15.6 |
| 1 | 11400 | 31.2 |

Therefore, it is concluded that the differences between measurements and calculations at each position can be considered as a random variable distributed normally. So the estimated standard deviation can be obtained from the samples for every cycles and burnup steps as shown in Fig. 9.

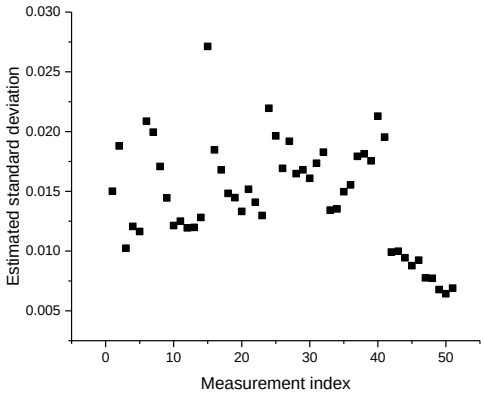


Fig. 9. Estimated standard deviations of the relative neutron flux differences between measurement data and calculated results for all cycles and burnup steps

If it's further assumed that all samples of each cycle and burnup step have the same population mean and variance, taking the average from the data given in Fig. 9 provides the mean value, 0.015, which stands for the estimated standard deviation of the difference between measurement and calculation.

## 4. Conclusion

The core follow calculation of Hanbit Unit 1 has been performed by using DeCART2D/MASTER codes system. The calculation results are compared with measurement data for the physical parameters such as CBC, ITC and reaction rates of incore detectors. As a result, the statistical parameters for estimating the calculation uncertainties are obtained for several important physical parameters such as CBC, ITC and relative neutron flux densities at various positions. It turns out that the maximum differences emerge as 55 ppm for CBC at ARO condition and -0.87 ppm/℃ for ITC, 466.1 pcm for HFP reactivity. In case of detector response, the standard deviation of the samples is calculated by 0.015, which is drawn from the observed samples at various cycles and burnup steps.

## REFERENCES

[1] J. Y. Cho, et al., "DeCART2D v1.1 User's Manual," KAERI/UM-40/2016, 2016.
[2] J. Y. Cho, et al., "MASTER v4.0 User's Manual," KAERI/UM-41/2016, 2016.
[3] J. S. Song, et al., "PROLOG1.1 User's Manual," KAERI/UM-4/99, 1999.
[4] C. B. Shim, et al., "Improvement of Axial Reflector Cross Section Generation Model for PWR Core Analysis," Transactions of the Korean Nuclear Society Autumn Meeting, Gyeongju, Korea, October 27-28, 2016.